JEE Journal of Ecological Engineering

Journal of Ecological Engineering, 2026, 27(2), 357–370
https://doi.org/10.12911/22998993/211658
ISSN 2299–8993, License CC-BY 4.0

Received: 2025.09.16
Accepted: 2025.12.15
Published: 2026.01.15

Performance of resin immobilized photocatalyst-TiO_2 in treating wastewater containing hexavalent chromium

Euis Nurul Hidayah[1*], Nur Laili Alfiatin Mukharomah[2]
Okik Hendriyanto Cahyonugroho[1], Ika Nawang Puspitawati[3],
Moch. Andy Wibisono[2], R Mohammad Alghaf Dienullah[1], Murat Yılmaz[4]

[1] Department of Environmental Engineering, Universitas Pembangunan Nasional Veteran Jawa Timur, Surabaya, 60294, Indonesia
[2] Environmental Research Center, Universitas Pembangunan Nasional Veteran Jawa Timur, Surabaya, 60294, Indonesia
[3] Department of Chemical Engineering, Universitas Pembangunan Nasional Veteran Jawa Timur, Surabaya, 60294, Indonesia
[4] Department of Chemistry and Chemical Processing Technologies, Bahçe Vocational School, Osmaniye Korkut Ata University, Osmaniye, 80000, Türkiye
* Corresponding author's e-mail: euisnh.tl@upnjatim.ac.id

ABSTRACT

Electroplating effluents are a significant source of toxic heavy metals, with hexavalent chromium being of particular concern due to its severe health hazards. This research investigates the efficiency of a Resin-Immobilized Photocatalyst (RIP-TiO_2) in removing Cr^{6+} from wastewater using a fixed-bed photocatalytic reactor. Experiments were carried out with both actual electroplating wastewater and synthetic wastewater, employing three RIP-TiO_2 dosages (30, 40, and 50 g) and sampling intervals of 0, 5, 15, 30, 45, 60, 75, 120, and 180 minutes. The reactor was operated with three column beds under UV-C irradiation (15 W). The study used two different types of media, electroplating wastewater (real wastewater) and synthetic wastewater (Cr^{6+} solution). The comparison initial Cr^{6+} concentrations measured were 1004.7 mg/L for real wastewater and 84.97 mg/L for synthetic wastewater. After 180 minutes of treatment with 50 g of RIP-TiO_2, removal efficiencies reached 70.67% for real wastewater and 37.64% for synthetic wastewater respectively. Datas were statistically evaluated using One-Way ANOVA followed by Tukey's test. The findings demonstrate that resin-supported TiO_2 effectively reduces Cr^{6+} levels, with optimal performance obtained under acidic pH and prolonged contact time.

Keywords: hexavalent chromium, photocatalysis, resin-immobilized TiO_2, electroplating wastewater, fixed-bed reactor.

INTRODUCTION

Recently, Industrial electroplating activities essentially produce various outputs, one of which is wastewater containing many heavy metals, such as cadmium (Cd), copper (Cu), zinc (Zn), mercury (Hg), chromium (Cr), lead (Pb), and others (Ayub et al., 2020). In the wide range, the production of electroplating wastewater is estimated to exceed 10 million tons per year, posing considerable environmental threats (Ma and Xiong, 2025). In nature, leaching, seepage, and diffusion processes can causing heavy metals in water to migrate into groundwater through soil layers (Wei et al., 2023). Heavy metals present severe risks and are highly hazardous to ecological systems especially human health (Elystia et al., 2021). The toxicity and stability effects of hexavalent chromium (Cr^{6+}) require special attention because they are harmful to living organisms (Suharjo et al., 2022). According to the World Health Organization (2017), the maximum concentration of chromium in water is 0.05 mg/L. In addition, due to the chemical stability of Cr^{6+} and

its toxicity level reported to be approximately 100 times higher than the trivalent form of chromium, which causes the permissible concentration of Cr^{6+} to be strictly limited. (Alvarez et al., 2021).

The development of efficient and effective wastewater treatment technologies is essential for reducing heavy metal concentrations in contaminated water. Among the available technologies, Advanced Oxidation Processes (AOPs) represent a promising option due to its degrade or eliminate pollutants through oxidative reactions. AOPs are chemical treatment methods specifically designed to decompose organic compounds in water and wastewater, thereby reducing chemical oxygen demand (COD), by generating highly reactive hydroxyl radicals (Wijayanti et al., 2023). AOPs have advantages over other methods, such as high degradation efficiency and the ability to break down persistent and toxic pollutants more effectively than conventional methods. Hydroxyl radicals, which are present in this process, can be generated through several techniques, such as photocatalysis, which is the most widely used technique (Shoneye et al., 2022).

Photocatalysis is a reaction process in which light energy (photons) activates semiconductor materials, such as titanium dioxide (TiO_2), to generate hydroxyl radicals that oxidize pollutants. TiO_2 has relatively wide band gap (3.0–3.2 eV), which enables it to absorb high-energy ultraviolet (UV) photons than other semiconductor (Rahman et al., 2019). Several previous research have demonstrated the effectiveness of TiO_2 in remove both inorganic and organic contaminants by photochemical reactions. Although the application of TiO_2 in powder form presents certain challenges, including difficulties in recovery after treatment and the potential risk of secondary contamination. Photocatalyst immobilization on resin has been proposed as an effective strategy to cover its limitation. This approach maintains the catalytic activity of TiO_2 in pollutant degradation while simplifying separation after the reaction (Zakria et al., 2021).

Photocatalysts are typically semiconducting materials capable of generating charge carriers when exposed to photons with energy equal to or greater than their band gap ($h\upsilon \geq Eg$) (Ramadhika et al., 2021). In photocatalysis, semiconductor catalysts such as TiO_2 are activated under UV-C irradiation to produce hydroxyl radicals (•OH), facilitating the reduction of Cr^{6+} to its less toxic Cr^{3+} form. The present study investigates the efficiency of resin-immobilized TiO_2 (RIP-TiO_2), supported on Dowex resin, for the photocatalytic reduction of Cr^{6+} in electroplating wastewater. The performance was evaluated using a multi-column continuous fixed-bed reactor with actual industrial effluent from electroplating processes, and results were directly compared with synthetic wastewater ($K_2Cr_2O_7$ solution) under identical operational conditions by varying catalyst dosage and sampling intervals.

The primary operational parameters considered in this study were those relevant to large-scale applications, including the influence of catalyst dosage on removal efficiency, pH variations, turbidity effects on UV penetration, and the likelihood of clogging within the fixed-bed system. Such parameters have seldom been comprehensively addressed in prior investigations of RIP-TiO_2. Earlier research on immobilized photocatalysts has largely focused on synthetic wastewater at lower contaminant concentrations and employed different supports or immobilization approaches – for instance, studies on immobilization techniques (Zakria et al., 2021), applications of photocatalyst resins to other parameters (Hidayah et al., 2022), and photocatalytic removal of Cr^{6+} and pigments (Kangralkar et al., 2021).

Only a limited number of studies have systematically evaluated photocatalyst performance in real wastewater with high contaminant concentrations under continuous fixed-bed reactor operation. To the best of our knowledge, this work represents the first direct comparison of RIP–TiO_2 performance between actual electroplating effluent containing elevated Cr^{6+} levels and synthetic wastewater in a continuous-flow fixed-bed system. The results highlight important scale-up considerations, including turbidity effects and reactor clogging, which have seldom been addressed in earlier research.

RESEARCH METHOD

The materials used in this study consisted of electroplating wastewater, synthetic wastewater (Cr^{6+} solution), TiO_2 semiconductor catalyst, Dowex resin, and deionized (DI) water. Prior to application, the resin was immobilized with TiO_2. The procedure resin immobilization process is shown in Figure 1 and the visualization of the RIPT-TiO_2 reactor used is shown in Figure 2.

The performance of RIP–TiO_2 in removing Cr^{6+} was evaluated by plotting the percentage

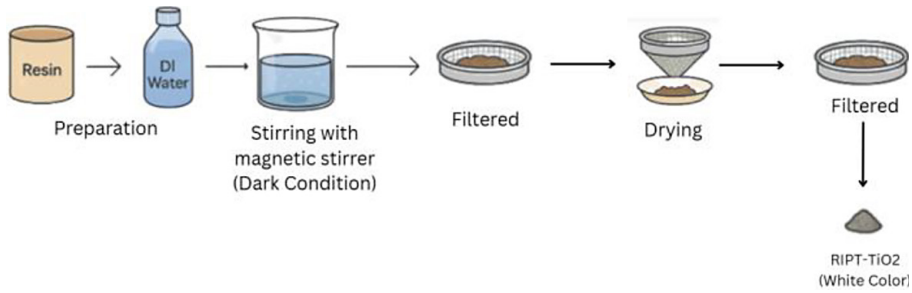

Figure 1. Procedure immobilization TiO_2

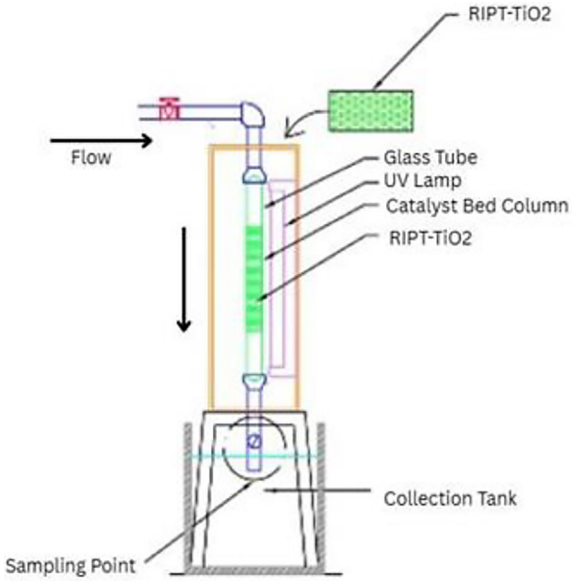

Figure 2. RIPT-TiO_2 reactor

of Cr^{6+} removal against different sampling times. Cr^{6+} concentration was measured in accordance with SNI 6989.71-2009, while turbidity was analyzed following SNI 06-6989.25-2005. Removal efficiency was expressed as the percentage reduction of Cr^{6+}. Statistical evaluation was performed using Minitab 17 (Free User) with the Two-Way ANOVA method to assess the influence of wastewater type, catalyst mass, and sampling time on removal efficiency. The statistical analysis specifically examined whether a significant difference existed in Cr^{6+} removal performance between real wastewater and synthetic wastewater. This comparison was emphasized as it distinguishes actual effluent conditions from controlled laboratory conditions, thereby forming the central focus of the study. Two-Way ANOVA was selected as it satisfies the underlying assumptions: the response variable (Cr^{6+} removal percentage) is quantitative, observations are independent, and although additional factors such as catalyst mass and contact time were considered, these were evaluated descriptively through trend analysis. Thus, the inferential hypothesis testing was primarily directed at comparing treatment effectiveness between real and artificial wastewater. The general research methodology is depicted in Figure 3.

The independent variables considered in this study were the type of wastewater (synthetic Cr^{6+} solution and electroplating effluent), RIP-TiO_2 catalyst dosage (30, 40, and 50 g), and sampling intervals (0, 5, 15, 30, 45, 60, 75, 120, and 180 minutes). Sampling was carried out in duplicate, constrained by the limited availability of real electroplating wastewater. The controlled variables included the type of immobilized resin, the initial Cr^{6+} concentration of the wastewater, and the reactor configuration (fixed-bed system). The research matrix listing the studied parameters is summarized in Table 1.

Initial characterization of the real wastewater revealed a Cr^{6+} concentration of 1004.7 mg/L, considerably exceeding regulatory limits. The turbidity was measured between 204 and 263 NTU, indicating a substantial presence of suspended solids, and the pH was 3.6, reflecting acidic conditions below the acceptable range. These findings demonstrate that real wastewater is highly polluted and unsuitable for direct environmental discharge. In comparison, artificial wastewater was prepared by adding potassium dichromate ($K_2Cr_2O_7$) to mimic the acidic pH of the original sample, which was adjusted to pH 3. Analysis of this artificial solution showed a Cr^{6+} concentration of 84.97 mg/L, markedly lower than that of the real wastewater. Moreover, the turbidity was minimal (0.64 NTU), while the pH of 3 confirmed acidic conditions outside the standard pH range of 6–9.

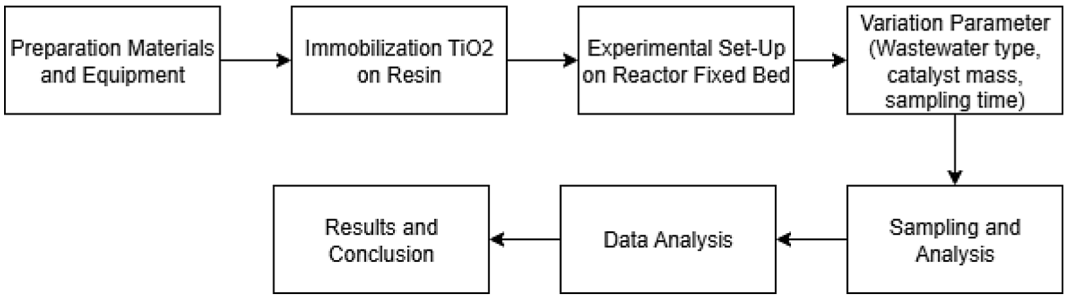

Figure 3. Research methodology

Table 1. The research matrix listing the studied parameters

Wastewater type	Resin immobilized mass (g)	Sampling time (min)	Code
Artificial Cr^{6+} solution	30	0-180	A
	40		B
	50		C
Electroplating effluent	30		D
	40		E
	50		F

RESULT AND DISCUSSION

The role of pH in photocatalyst effectiveness

The pH of a solution is a critical parameter influencing photocatalyst performance, particularly for TiO_2. The activity of TiO_2 is strongly affected by the initial solution pH, which significantly determines its crystal phase (anatase, rutile, or a combination), crystallite size, and overall morphology (Yalcin, 2022). The solution's acidity also governs electrostatic interactions at the catalyst surface, as explained by the concept of the isoelectric point (IEP). When the pH approaches the IEP, the zeta potential of TiO_2 approaches zero, weakening repulsive forces between particles and promoting agglomeration (Gomez-Polo et al., 2021). This aggregation reduces the catalyst's active surface area, thereby lowering photocatalytic efficiency. Previous studies indicate that unmodified TiO_2 exhibits an IEP between pH 4.5 and 5.5 (Wang et al., 2021), whereas modified TiO_2 can have an IEP around pH 4.2 (Zare et al., 2021). Consequently, the initial pH of wastewater is a key factor that influences the effectiveness of the photocatalysis process (Al-Nuaim et al., 2023).

In the fixed-bed reactor experiments with artificial wastewater, RIP-TiO_2 catalyst masses of 30, 40, and 50 g were employed. As presented in Figure 4a, all conditions began with the same initial pH of 3 at time zero, confirming uniform starting conditions. Within the first 5 minutes of treatment, the pH decreased across all dosages, reaching 1.8 for the 30 g and 40 g variations, while the 50 g dosage exhibited a slightly higher value of 1.9. This rapid decline is attributed to ionization processes and the early interaction between the TiO_2 photocatalyst and H^+ ions in the medium, which increases proton concentration and consequently lowers the pH.

Between 15 and 45 minutes, the pH values remained nearly constant across all catalyst dosages, with 1.8 recorded for the 30 g and 40 g masses, and 1.8–1.9 for the 50 g mass. This stability suggests that the majority of H^+ ions generated during the initial stage had reached equilibrium, while the reduction of Cr^{6+} to Cr^{3+} continued at a steady rate. At 60 and 75 minutes, slight variations were observed among the different dosages: the 30 g mass showed a decline to pH 1.7, the 40 g mass remained at 1.8, and the 50 g mass maintained stability at 1.8. These differences can be attributed to variations in adsorption capacity and surface area of the TiO_2 catalyst, with the higher dosages (40 and 50 g) providing greater capacity to regulate H^+ ion concentration.

At 120 and 180 minutes, more pronounced variations in pH were observed among the different catalyst dosages. The 30 g mass showed a further decline to 1.7, whereas the 40 g mass dropped more substantially, reaching 1.4 at 120

minutes and 1.0 at 180 minutes. In contrast, the 50 g mass maintained stability at 1.8 throughout this period. These trends suggest that at the lower dosage (30 g), the limited amount of catalyst restricts H^+ adsorption, leading to the accumulation of protons in solution as the Cr^{6+} reduction progresses. The sharper decrease with 40 g may reflect a stronger photocatalytic activity, where the reduction of Cr^{6+} generates more H^+ ions than the system can buffer. By comparison, the 50 g mass exhibited superior pH stability, likely due to the higher quantity of TiO_2 providing greater capacity to adsorb H^+ ions and preserve surface electrostatic balance.

In this study, the real wastewater had an initial pH of 3.6, whereas the artificial wastewater was prepared at pH 3 to mimic the acidic conditions of the real sample (Figure 4b). This low pH was selected because the behavior of Cr^{6+} ions is highly dependent on the solution's acidity. During photocatalysis in a fixed-bed reactor, the pH of both wastewaters varied due to the reduction of Cr^{6+} to Cr^{3+}, which releases H^+ ions into the solution (Gao and Meng, 2021). The reduction of Cr^{6+} requires both electrons and protons, with electrons provided by semiconductor excitation under light irradiation and H^+ ions readily available under acidic conditions. This explains why Cr^{6+} reduction is more efficient at low pH compared to alkaline environments. Consistently, Kangralkar et al. (2021) reported that the highest degradation efficiencies are observed under acidic conditions, decreasing as the solution becomes more alkaline.

An interesting condition to note is the final pH value or pH of the sample after passing through the photocatalytic reactor. In electroplating waste, the pH value fluctuates significantly over a period of up to 180 minutes, while in artificial waste it remains fairly constant up to 180 minutes. In electroplating waste, there is an increase from pH 3.6 to 4.5 and then a decrease to 3.2. In contrast, artificial waste shows a significant decrease from pH 3 to a range of 1.7–1.8. This significant decrease is possible due to the photocatalytic reaction itself, which produces H+ ions that can lower the pH value of the solution. This can be explained by the following reaction equation (Navidpour et al., 2023):

$$Semikonduktor + h\vartheta \rightarrow \rightarrow Semikonduktor\ (h^+{}_{VB} + e^-{}_{CB}) \quad (1)$$

$$h^+{}_{VB} + e^-{}_{CB} \rightarrow heat\ (energy) \quad (2)$$

$$H_2O + h^+{}_{VB} \rightarrow \cdot OH + H^+ \quad (3)$$

From the reaction equation, it can be seen that the photocatalytic process produces holes (h^+) that react with water to form H^+ ions. Artificial waste itself only contains water and Cr^{6+} ions from dissolved potassium dichromate ($K_2Cr_2O_7$). This is different from electroplating waste, which contains other substances or compounds. According to (Riahi et al., 2022), electroplating waste can contain alkalinity in the form of $CaCO_3$, organic materials, and other heavy metals. This may indicate the presence or absence of a pH buffer system that can maintain the pH of the solution so that it does not change significantly when undergoing a process or reaction. In electroplating waste, the buffer can be carbonate ions (CO_3^{2-}) from alkalinity in the form of $CaCO_3$. These ions will react with the H^+ ions formed so that the pH of the sample will not drop significantly. Artificial waste itself does not contain other substances or compounds, so it does not have buffer capacity, allowing its pH to drop significantly.

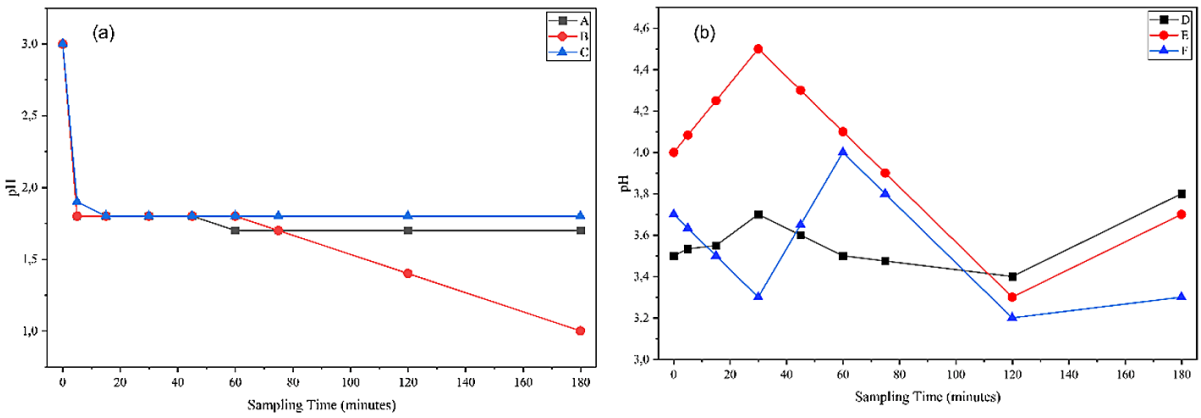

Figure. 4. The pH change of a) artificial wastewater (A: 30 g, B: 40 g, C: 50 g), b) real wastewater (D: 30 g, E: 40 g, F: 50 g)

Suspended particles and photocatalyst performance

Wastewater with high turbidity contains numerous suspended solids that hinder light penetration (Suhendara et al., 2020). This limitation reduces the efficiency of photocatalyst activation, as effective photocatalysis requires adequate light exposure. Furthermore, the particles responsible for turbidity may adhere to the photocatalyst surface, masking active sites and diminishing catalytic performance. As a consequence, the reduction of Cr^{6+} to Cr^{3+} is suppressed, leading to lower overall removal efficiency. In both real wastewater and synthetic solutions, turbidity gradually decreased with treatment time (0, 5, 15, 30, 45, 60, 75, 120, and 180 minutes), as illustrated in Figure 5.

In artificial wastewater, the initial turbidity was relatively low, measured at 0.64 NTU for all catalyst dosages. This suggests the absence of suspended solids, complex organic matter, or heavy metals other than Cr^{6+} that could contribute to turbidity. As shown in Figure 2(a), turbidity increased at the 5-minute mark across all RIP–TiO_2 dosages, with the highest value recorded for 50 g (8.78 NTU), followed by 40 g (3.24 NTU) and 30 g (2.59 NTU). This rise was attributed to the leaching of TiO_2 particles from the resin, which elevated the particle concentration in solution. With continued treatment, turbidity levels progressively declined, ultimately dropping below the initial values. The lowest turbidity was observed at 180 minutes for both the 50 g and 30 g dosages (0.16 NTU), while the 40 g dosage reached its minimum (0.25 NTU) at 60 minutes. In terms of turbidity removal efficiency, the 50 g and 30 g dosages achieved the highest reduction of 75% at 180 minutes, whereas the 40 g dosage reached 60.94% at 60 minutes. The enhanced performance of the 40 g dosage at earlier stages may be linked to sufficient generation of reactive radicals (•OH and $O_2•^-$), which accelerated pollutant degradation and resulted in a faster reduction of turbidity.

Turbidity in wastewater is typically attributed to suspended solids, complex organic matter, or heavy metals other than Cr^{6+}. As illustrated in Figure 5(b), turbidity gradually declined during treatment in the fixed-bed reactor. By 180 minutes, the lowest turbidity level was observed with the 50 g RIP-TiO_2 dosage (15.5 NTU), followed by the 40 g (44.2 NTU) and 30 g (56.1 NTU) dosages. In terms of removal efficiency, the 50 g mass achieved the highest reduction at 92.4%, whereas the 40 g and 30 g masses reached 78.44% and 78.67%, respectively.

Performance of RIP-TiO_2 in Cr^{6+} removal

The results presented in Figure 6 indicate that Cr^{6+} removal gradually increases with higher RIP–TiO_2 dosages and longer reaction times. At the beginning of the process (0 min), the removal efficiency was minimal, but it progressively rose at 5, 15, 30, 45, 60, 75, and 120 min, achieving the maximum efficiency at 180 min. This trend can be explained by the fact that activation of the photocatalyst surface under irradiation is not immediate; a certain duration is necessary for the consistent generation of hydroxyl radicals (•OH) (Chakravorty and Roy, 2024). Such behavior aligns with the principles of heterogeneous photocatalysis, which state that a newly introduced catalyst attains stable activity only after reaching a steady-state condition (Arinda et al., 2025). Accordingly, the surface of the photocatalyst must

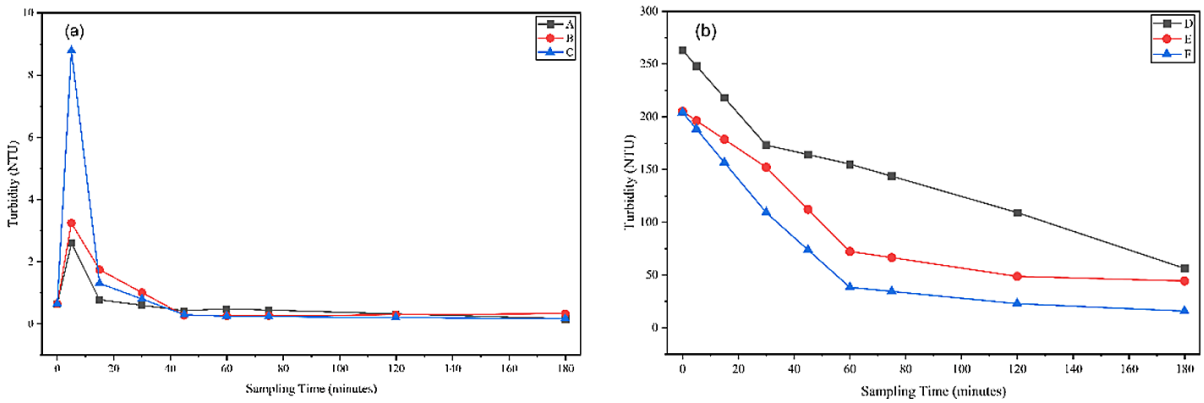

Figure 5. Turbidity concentration of a) artificial wastewater (A: 30 g, B: 40 g, C: 50 g), b) real wastewater (D: 30 g, E: 40 g, F: 50 g)

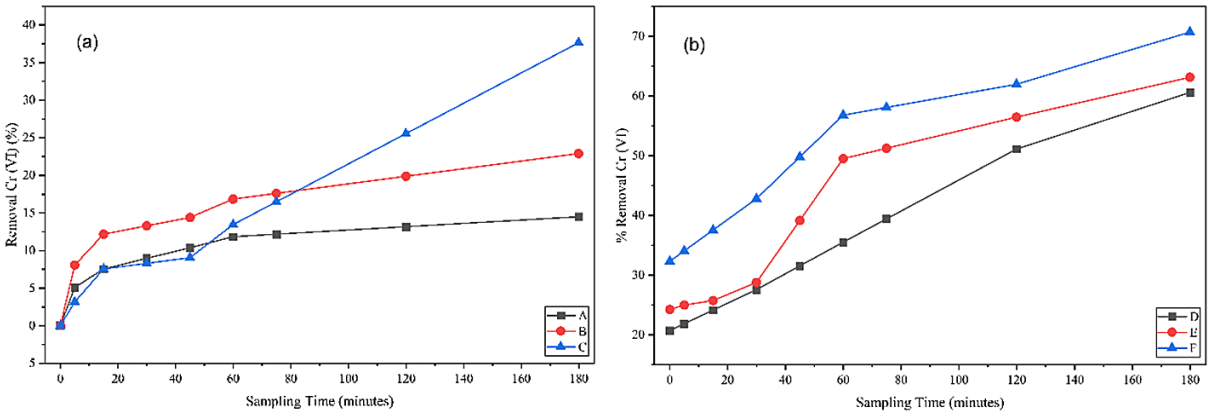

Figure 6. Percentage of Cr^{6+} removal from artificial wastewater (A: 30 g, B: 40 g, C: 50 g), b) real wastewater (D: 30 g, E: 40 g, F: 50 g)

undergo a response period under irradiation before its performance stabilizes.

At the initial stage of the reaction, RIP–TiO_2 exhibits limited photocatalytic activity, leading to low Cr^{6+} removal efficiency. The reduction of Cr^{6+} to Cr^{3+} becomes more pronounced, it showed from the higher removal performance (Song et al., 2022). Based form overall efficiency, photocatalytic efficiency is strongly dependent on the intrinsic characteristics of the semiconductor employed. TiO_2 is considered an excellent option photocatalyst due to its chemical stability, low cost, non-toxicity, and favorable electronic. Specifically, electrons excited into the conduction band of TiO_2 can interact with dissolved oxygen to form superoxide radicals ($O_2^{\bullet-}$), which enhance the degradation process (Shoneye et al., 2022). Because of the attributes, TiO_2 has found wide application such as in catalytic processes, mineral membranes, dielectric materials, and environmental remediation. TiO_2 occurs in three major crystalline forms – anatase, rutile, and brookite – with band gap energies of 3.2, 3.0, and 3.1 eV, respectively (Navidpour et al., 2023).

Figure 6a illustrates that the percentage of Cr^{6+} removal in artificial wastewater increased progressively during photocatalysis. At the beginning of the process, the inlet Cr^{6+} concentration was 84.97 mg/L. After 180 minutes of treatment with different RIP–TiO_2 dosages, a notable enhancement in removal efficiency was observed. Using 30 g of catalyst, Cr^{6+} removal reached 14.47% (72.68 mg/L remaining), while 40 g achieved 22.88% (65.53 mg/L remaining). The highest performance was obtained with 50 g of RIP–TiO_2, corresponding to 37.64% removal and a residual concentration of 52.99 mg/L.

Figure 6b shows that Cr^{6+} removal in real wastewater increased throughout the photocatalysis process. At the start, the inlet Cr^{6+} concentration was 1004.7 mg/L. Following 180 minutes of treatment with varying RIP–TiO_2 dosages, the removal efficiency increased substantially. Using 30 g of catalyst, Cr^{6+} removal reached 60.56%, corresponding to a residual concentration of 396.30 mg/L. With 40 g, the removal improved to 63.09% (370.80 mg/L remaining), while the highest efficiency of 70.67% was achieved with 50 g, leaving 299.70 mg/L of Cr^{6+}.

In addition to electroplating wastewater, artificial wastewater was employed in this study to evaluate the consistency of photocatalyst performance under controlled conditions. Potassium dichromate ($K_2Cr_2O_7$) was used to prepare artificial wastewater containing Cr^{6+}, which exhibited a bright orange color, no detectable odor, and an acidic pH. The aim of the treatment process was to reduce hexavalent chromium (Cr^{6+}) via photocatalysis. During this reduction, Cr^{6+} is converted into trivalent chromium (Cr^{3+}), which is less toxic and environmentally safer. The following section presents the results of Cr^{6+} removal in the artificial wastewater system.

The removal of Cr^{6+} using TiO_2 under different conditions has also been investigated in previous studies. For instance, Kangralkar et al. (2021) reported that photocatalysis with ZnO under UV irradiation achieved up to 65% Cr^{6+} removal; however, their experiments were limited to artificial wastewater with an initial Cr^{6+} concentration below 100 mg/L, which is comparatively low. Similarly, Song et al. (2022) demonstrated a maximum Cr^{6+} removal efficiency of 60% using a TiO_2-based micro-nano reactor,

although this system was tested only in a controlled artificial matrix.

In comparison with the previous studies, the present work achieved a higher Cr^{6+} removal efficiency of up to 70.67%, even when treating real wastewater with an initial concentration as high as 1004.7 mg/L. These results suggest that the immobilized resin configuration enhances stability against turbidity and interference from complex ions in real wastewater, while also facilitating catalyst recovery. Navidpour et al. (2023) observed and find the different between artificial and real wastewater artificial systems, the result showed that the performance of TiO_2 photocatalysis is strongly influenced by operational factors such as pH, turbidity, and ionic competition. Therefore, the findings of this study extend previous knowledge by demonstrating the new exploration of treating high-concentration industrial wastewater practical applicability of RIP–TiO_2.

Characterization of functional groups and BET analysis

The FTIR analysis results in Figure 7 show a broad band in the 3200–3550 cm^{-1} region, categorized as O–H stretching vibration from a hydrogen-bonded hydroxyl group. The peak absorption occurs at a wavelength of 3200–3500 cm^{-1}, indicating the presence of O–H stretching (Fanani and Ulfindrayani, 2019). In Figure 7, the FTIR spectrum of resin (a) and RIPT-TiO_2 (b) shows this broad band in the region of 3200–3600 cm^{-1} with q peak at 3456.44 cm^{-1} for resin with a transmittance intensity of approximately 58.47%. After immobilization with TiO_2, the band shifted to 3390.86 cm^{-1} with transmittance increasing to 78.47%. The shift of the q peak to a lower wave number indicates the formation of stronger hydrogen bonds between OH groups in the resin and the TiO_2 surface. Meanwhile, the increase in transmittance indicates a decrease in the number of free –OH groups capable of absorbing infrared radiation, as most of the –OH groups are involved in interactions with TiO_2.

After the use of RIPT-TiO_2 with artificial waste in Figure 7(c), the –OH band experienced a decrease in intensity with peak q at 3508.52 cm^{-1} along with transmittance increase to 88.88%. This indicates a reduction in hydroxyl groups, either due to involvement in reduction reactions or because they were covered by Cr species on the photocatalyst surface. This condition is consistent with the low Cr^{6+} removal efficiency, namely 14.47% (72.68 mg/L) at 30 g, 22.88% (65.53 mg/L) at 40 g, and 37.64% (52.99 mg/L) at 50 g. In contrast, the RIPT-TiO_2 used for electroplating waste in Figure 8, the –OH band detected with peak q at 3444.87 cm^{-1} and a transmittance of 64.44%. The relatively high presence of –OH groups indicates that the photocatalyst surface still provides active sites for Cr^{6+} ion adsorption and hydroxyl radical (•OH) formation. This is in line with the much higher Cr^{6+} removal efficiency, namely 60.56% (396.30 mg/L) at 30 g, 63.09% (370.80 mg/L) at 40 g, and 70.67% (299.70 mg/L) at 50 g. Thus, the presence of hydroxyl groups plays an important role in accelerating the reduction of Cr^{6+} to Cr^{3+} through the mechanism:

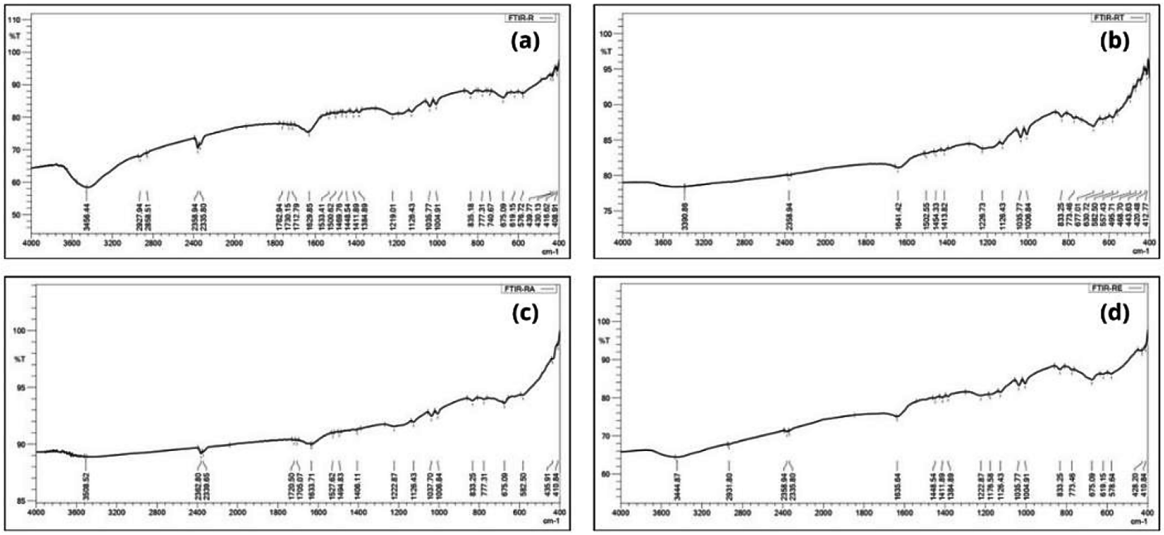

Figure 7. (a) resin (b) RIPT-TiO_2, (c) RIPT-TiO_2 on artificial Cr^{6+} waste (d) RIPT-TiO_2 on real wastewater

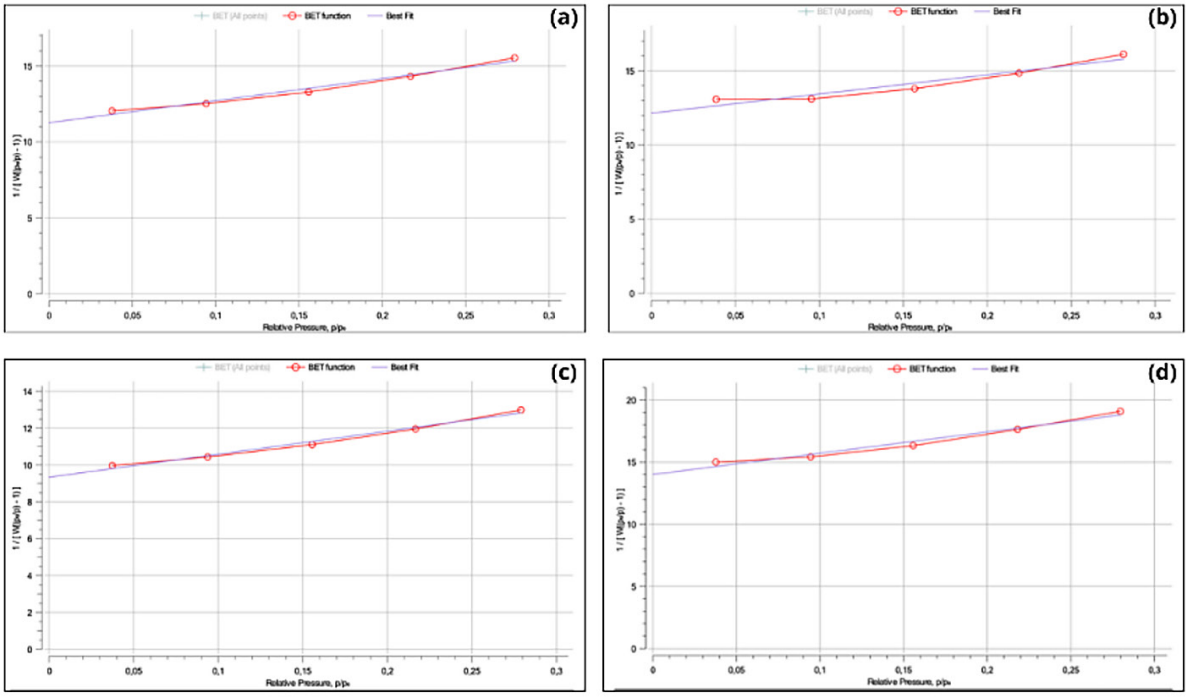

Figure 8. Multipoint BET graph: (a) resin, (b) RIPT-TiO_2, (c) RIPT-TiO_2 in artificial Cr^{6+} waste, (d) RIPT-TiO_2 in real wastewater

Several important properties such as specific surface area, pore size, and pore volume were analyzed using the Brunauer, Emmett and Teller (BET) method. The multipoint BET graph in the Figure 8 shows more accurate surface area calculations compared to single point. From the multipoint BET analysis, it is known that the correlation coefficient (R) value for the four samples is in the range of 0.960–0.992. The highest R value was obtained in the RIPT-TiO_2 sample in artificial Cr^{6+} waste code (c) of 0.992, followed by Resin code (a) of 0.989, and RIPT-TiO_2 sample in electroplating waste code (d) at 0.983, while the RIPT-TiO_2 sample code (b) at 0.960 had the lowest value. In general, an R value > 0.95 indicates that the analysis results are reliable and suitable for calculating specific surface area.

The adsorption isotherm results show that all samples have a characteristic curve of mesoporous material (type IV isotherm according to IUPAC classification), marked by an increase in adsorption volume as the relative pressure increases in the range of 0–0.3 p/p_0. This is consistent with the specific surface area (SA) data, which ranges from 111.8 to 159.5 m^2/g, generally associated with a mesoporous structure. The highest adsorption volume was observed in the RIPT-TiO_2 sample on artificial Cr^{6+} waste, in line with the largest SA value (159.5 m^2/g), which indicates the highest number of active pore sites for interaction with Cr^{6+} ions. Conversely, the RIPT-TiO_2 sample in electroplating waste showed the lowest adsorption volume, consistent with the lowest SA value (111.8 m^2/g), indicating limited adsorption capacity.

When related to photocatalytic performance, the surface area and isotherm shape explain the potential adsorption capacity of each sample, but are not the only factors determining removal efficiency. Although RIPT-TiO_2 in artificial Cr^{6+} waste had the highest SA, its removal efficiency was lower in the artificial waste test (14.47–37.64%), because the artificial system only contained single Cr^{6+} without additional electron donors. Conversely, RIPT-TiO_2 in electroplating waste with the lowest SA actually showed the highest removal efficiency (60.56–70.67%) in electroplating waste, which can be explained by the presence of other metal ions (Fe^{2+}, Cu^{2+}, Ni^{2+}) and organic compounds in real waste that act as additional reducing agents and suppress electron-hole recombination. Thus, the isotherm and SA results from BET analysis provide an overview of the adsorption capacity, while the composition of the actual waste matrix greatly affects the effectiveness of utilizing active sites on the photocatalyst surface (Licona-Aguilar et al., 2024).

Kinetics of hexavalent chromium reduction reactions

Kinetics is one of the interesting aspects to analyze in the photocatalysis process. Immobilized TiO_2 photocatalyst resin is a solid semiconductor used in the photocatalysis process to reduce Cr^{6+} in this study. This means that a heterogeneous photocatalysis process (solid semiconductor and liquid sample) occurs. The Langmuir-Hinshelwood kinetic model is commonly used to observe the reaction kinetics that occur in heterogeneous photocatalysis processes (Table 2). The Langmuir-Hinshelwood model can be written as follows (Tran et al., 2023):

$$-\frac{dC_a}{dt} = \frac{k_{deg}KC_a}{1+KC_a} \quad (4)$$

$$-\frac{dC_a}{dt} = k_n {C_a}^n \quad (5)$$

Equation 2 is a pseudo-order kinetic model, if:

$$k_{ap} = \frac{k_{deg}KC_a}{1+KC_a} \quad (6)$$

$$-\frac{dC_a}{dt} = k_{ap}C_a \quad (7)$$

Equation 4 is the same as Equation 2 when the value of n is 1, or it can be interpreted as the pseudo first order model. When the order is 1, the kinetic model can be written as follows:

$$ln\frac{C_{a0}}{C_a} = kt \quad (8)$$

The reaction constant value (k) can be obtained by plotting a graph between the time value (t) on the x-axis and the value $ln\frac{C_{a0}}{C_a}$ on the y-axis. The graph is as follows:

Figure 9 shows a graph plot for the Langmuir-Hinshelwood (L-H) kinetic model simplified into Pseudo-First Order (PFO). The figure shows an increase over a time range of up to 180 minutes. In addition, a catalyst mass of 50 grams has a higher value. The results obtained show that the R^2 value for real wastewater decreases as the catalyst mass increases. From this, it can be said that the PFO model is quite good at describing the kinetics at a catalyst mass of 30 grams, but its accuracy decreases as the catalyst mass increases. Catalyst agglomeration and UV irradiation levels can cause this decrease, so that the Cr^{6+} reduction rate as the catalyst mass increases is not only influenced by the Cr^{6+} concentration. However, it can be seen that the reaction constant value increases with increasing catalyst mass, which means that the reaction rate that occurs with the addition of catalyst mass will be

Table 2. Kinetic model using RIPT-TiO_2 in electroplating and artificial wastewater

Wastewater type	Catalyst mass	R^2	k (min^{1-})
Electroplating	30	0.9415	0.00447
	40	0.8615	0.00495
	50	0.81924	0.00549
Artificial	30	0.6916	0.0007
	40	0.7621	0.0011
	50	0.9845	0.0025

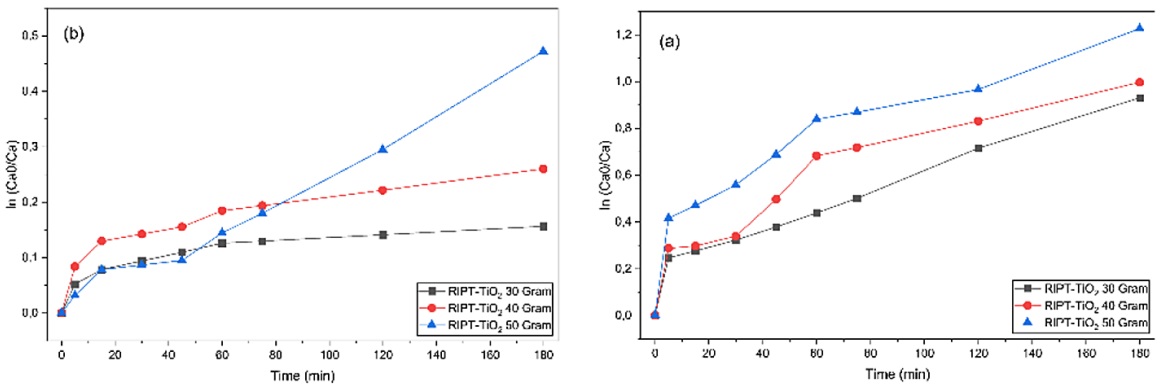

Figure 9. Langmuir-Hinshelwood kinetic model by approaching pseudo first order kinetic model in: a) real wastewater, b) artificial wasterwater

greater or increase. The theory of an increasing number of active catalyst sites or an increasing catalyst surface area with the addition of catalyst mass supports this pattern.

Conversely, in artificial waste, the R_2 value increases with the addition of catalyst mass, which means that the PFO model can accurately describe the reaction kinetics in artificial waste with a catalyst mass of 50 grams. Catalyst masses of 30 and 40 grams showed fairly low R^2 values, indicating that the L-H model with the PFO kinetic model approach was insufficient to describe the reaction kinetics occurring in these two variations. However, one thing that is the same as electroplating waste is that the reaction constant (k) also increases with the addition of catalyst mass, so that the reaction rate also increases with the addition of catalyst in the photocatalysis process.

Comparison of photocatalysis performance statistics in real wastewater and artificial wastewater

To learn more about the relationship between variables in the removal or reduction of hexavalent chromium in waste and the changes in pH that occur, a multi-factor ANOVA test in the form of a two-way ANOVA was conducted. The two-way ANOVA test data is as follows, consisting of the variables of waste type, catalyst mass, and sampling time (Figure 10).

From the Figure 11, it can be seen that the P-Value for the variation in waste type and the interaction between waste type and time is less than the rejection region (α = 5%), so it can be said that these variations have significant differences. This includes the interaction between waste type and catalyst mass and the interaction between waste type and time, both of which have significant differences. To explain this, a post-hoc test is required, while for the results of the interaction between catalyst mass and time, a post-hoc test is not required because the p-value is greater than the rejection region (α), so it can be said that the interaction between the two does not have a significant difference. The post-hoc test results are presented in Figure 12.

In the interaction between waste types and catalyst mass, it can be seen that the two waste types are in different groups, so that their removal in all types of catalyst mass shows significant differences. In addition, in the case of natural waste (code 1), the use of 50 grams of catalyst mass shows a significant difference compared to 30 and 40 grams of catalyst mass,

Factor Information

Factor	Type	Levels	Values
Wastewater Type	Fixed	2	1; 2
Catalyst Mass	Fixed	3	30; 40; 50
Time	Fixed	9	0; 5; 15; 30; 45; 60; 75; 120; 180

Figure 10. Two-way ANOVA test data

Analysis of Variance

Source	DF	Adj SS	Adj MS	F-Value	P-Value
Wastewater Type	1	11528,7	11528,7	649,19	0,000
Catalyst Mass	2	797,5	398,7	22,45	0,000
Time	8	5371,1	671,4	37,81	0,000
Wastewater Type*Catalyst Mass	2	299,1	149,5	8,42	0,003
Wastewater Type*Time	8	613,0	76,6	4,31	0,006
Catalyst Mass*Time	16	155,0	9,7	0,55	0,882
Error	16	284,1	17,8		
Total	53	19048,4			

Figure 11. ANOVA-Two test results

Wastewater Type*Catalyst Mass

	N	Mean	Grouping
1 50	9	49,2963	A
1 40	9	40,3089	B
1 30	9	34,6671	B
2 40	9	13,8876	C
2 50	9	13,4437	C
2 30	9	9,2724	C

Means that do not share a letter are significantly different.

Wastewater Type*Time

	N	Mean	Grouping
1 180	3	64,7722	A
1 120	3	56,4713	A B
1 75	3	49,5388	A B C
1 60	3	47,2280	B C D
1 45	3	40,1131	C D E
1 30	3	32,9982	D E F
1 15	3	29,0922	E F G
1 5	3	26,9102	E F G H
1 0	3	25,6926	E F G H I
2 180	3	24,9961	E F G H I
2 120	3	19,5114	F G H I J
2 75	3	15,3980	G H I J K
2 60	3	14,0268	G H I J K
2 45	3	11,2530	H I J K
2 30	3	10,1576	I J K
2 15	3	9,0623	J K
2 5	3	5,4058	J K
2 0	3	-0,0000	K

Means that do not share a letter are significantly different.

Figure 12. ANOVA-Two Post-Hoc test results

while in the case of artificial waste, there is no difference in the use of all types of catalyst mass. From this, it can be said that in original waste, differences in catalyst mass usage will result in significant differences in Cr^{6+} removal, with the optimum removal level obtained with a catalyst mass of 50 grams, while in artificial waste, differences in catalyst mass do not result in significantly different removal levels.

Then, in the interaction between waste types and time, there is a visible interaction between the two. Original waste (code 1) is visible in the time variation interval in several different groups. This indicates that there are differences in removal in each given time interval. However, artificial waste (code 2) is seen in the same group in each time interval. This indicates that the removal between the given time intervals is not much different. From this, it can be said that real wastewater has a different removal rate at each time and tends to increase, with the highest average at 180 minutes.

CONCLUSIONS

The results of this study demonstrate that photocatalysis using RIP–TiO_2 in a fixed-bed reactor effectively reduces Cr^{6+} concentrations, with removal efficiency increasing as both the photocatalyst mass and contact time increase. For instance, a maximum Cr^{6+} removal of 70.67% was achieved using 50 g of catalyst after 180 minutes, whereas artificial wastewater exhibited a lower maximum removal of 37.64%. Turbidity removal was also notable, reaching 92.40% in real wastewater and 75% in artificial wastewater, highlighting the effectiveness of RIP-TiO_2, particularly in treating more complex electroplating effluents.

These findings indicate that photocatalysis with RIP–TiO_2 in a fixed-bed configuration holds promise for industrial-scale treatment of real wastewater containing high concentrations of heavy metals and acidic pH. Nevertheless, this study has some limitations. The surface characteristics of the immobilized resin were not characterized, leaving uncertainties regarding its stability and morphology. Additionally, the experiments were conducted at the laboratory scale, so further investigation is needed to assess the long-term durability of the material, resin regeneration, and the effects of other interfering ions present in real wastewater.

Acknowledgements

This study was financially supported by Directorate General of Research and Development, Ministry of Higher Education, Science and Technology, SP 9/UN63.8/LT – Contract/VI/2025, June 5th, 2025.

REFERENCES

1. Al-Nuaim, M. A., Alwasiti, A. A., Shnain, Z. Y. (2023). The photocatalytic process in the treatment of polluted water. In *Chemical Papers* 77(2), 677–701. Versita. https://doi.org/10.1007/s11696-022-02468-7
2. Alvarez, C. C., Bravo Gómez, M. E., Hernández Zavala, A. (2021). *Hexavalent chromium*: Regulation and health effects. *Journal of Trace Elements in Medicine and Biology*, *65*, 126729. https://doi.org/https://doi.org/10.1016/j.jtemb.2021.126729
3. Arinda, E., Hidayah, E. N., Dienullah, R. M. A., Yilmaz, M. (2025). Impact of ultraviolet light spacing and fixed zinc oxide resin on total nitrogen and phosphate removal in a continuous photocatalytic reactor. *Journal of Ecological Engineering*, *26*(9), 449–458. https://www.jeeng.net/Impact-of-ultraviolet-light-spacing-and-fixed-zinc-oxide-resin-on-total-nitrogen,205346,0,2.html
4. Ayub, S., Siddique, A. A., Khursheed, M. S., Zarei, A., Alam, I., Asgari, E., Changani, F. (2020). Removal of heavy metals (Cr, Cu, and Zn) from electroplating wastewater by electrocoagulation and adsorption processes. *Desalination and Water Treatment*, *179*(3), 263–271. https://doi.org/10.5004/dwt.2020.25010
5. Chakravorty, A., Roy, S. (2024). A review of photocatalysis, basic principles, processes, and materials. *Sustainable Chemistry for the Environment*, *8*(8), 1–18. https://doi.org/10.1016/j.scenv.2024.100155
6. Elystia, S., HS, E., Karamy, A. G. (2021). Penyisihan logam Cr (VI) dari limbah cair elektroplating menggunakan mikroalga *Chlorella* sp. dengan variasi penambahan external-glutathione. *Jurnal Serambi Engineering*, *6*(1), 1522–1528. https://doi.org/10.32672/jse.v6i1.2606
7. Fanani, N., Ulfindrayani, I. F. (2019). Synthesis of activated carbon (ac) from bamboo waste as a support of zinc oxide (ZnO) catalyst. *Konversi*, *8*(2), 108–112. https://doi.org/10.20527/k.v8i2.7183
8. Gao, X., Meng, X. (2021). Photocatalysis for heavy metal treatment: A review. *Processes*, *9*(10), 2–12. https://doi.org/10.3390/pr9101729
9. Gomez-Polo, C., Larumbe, S., Gil, A., Muñoz, D., Fernández, L. R., Barquín, L. F., García-Prieto, A., Fdez-Gubieda, M. L., Muela, A. (2021). Improved photocatalytic and antibacterial performance of Cr doped TiO_2 nanoparticles. *Surfaces and Interfaces*, *22*, 100867.
10. Hidayah, E. N., Pachwarya, R. B., Cahyonugroho, O. H. (2022). Immobilization of resin photocatalyst in removal of soluble effluent organic matter and potential for disinfection by-products. *Global Journal of Environmental Science and Management*, *8*(3), 437–448. https://doi.org/10.22034/gjesm.2022.03.10
11. Kangralkar, M. V., Manjanna, J., Momin, N., Rane, K. S., Nayaka, G. P., Kangralkar, V. A. (2021). Photocatalytic degradation of hexavalent chromium and different staining dyes by ZnO in aqueous medium under UV light. *Environmental Nanotechnology, Monitoring & Management*, *16*(April), 100508. https://doi.org/10.1016/j.enmm.2021.100508
12. Licona–Aguilar, A. I., Torres–Huerta, A. M., Domínguez–Crespo, M. A., Negrete–Rodríguez, M. L. X., Conde–Barajas, E., Brachetti–Sibaja, S. B., Rodríguez–Salazar, A. E. (2024). Valorization of agroindustrial orange peel waste during the optimization of activated carbon–multiwalled carbon nanotubes–zinc oxide composites used in the removal of methylene blue in wastewater. *Chemical Engineering Journal*, *492*, 152102. https://doi.org/https://doi.org/10.1016/j.cej.2024.152102
13. Ma, J., Xiong, Z. (2025). Sustainable metal recovery from electroplating sludge: Bridging technology and environmental regulation. *Sustainability (Switzerland)*, *17*(11), 1–21. https://doi.org/10.3390/su17114957
14. Navidpour, A. H., Abbasi, S., Li, D., Mojiri, A., Zhou, J. L. (2023). Investigation of advanced oxidation process in the presence of TiO_2 semiconductor as photocatalyst: Property, principle, kinetic analysis, and photocatalytic activity. *Catalysts*, *13*(232), 1–29. https://doi.org/10.3390/catal13020232
15. Rahman, Z. U., Wei, N., Feng, M., Wang, D. (2019). TiO2 hollow spheres with separated Au and RuO_2 co-catalysts for efficient photocatalytic water splitting. *International Journal of Hydrogen Energy*, *44*(26), 13221–13231. https://doi.org/10.1016/j.ijhydene.2019.03.176
16. Ramadhika, L. N., Aprilia, A., Safriani, L. (2021). Studi preparasi senyawa ZnO:TiO_2 sebagai material fotokatalis. *Jurnal Material Dan Energi Indonesia*, *11*(02), 83–95.
17. Shoneye, A., Sen Chang, J., Chong, M. N., Tang, J. (2022). Recent progress in photocatalytic degradation of chlorinated phenols and reduction of heavy metal ions in water by TiO_2-based catalysts. *International Materials Reviews*, *67*(1), 47–64. https://doi.org/10.1080/09506608.2021.1891368
18. Song, Y., Lu, X., Liu, Z., Liu, W., Gai, L., Gao, X., Ma, H. (2022). *Efficient Removal of Cr (VI) by TiO_2 Based Micro-Nano Reactor via the Synergy of Adsorption and Photocatalysis*. *Vi*, 1–15.
19. Suharjo, M. H., Ernawati, R., Nurkhamim. (2022). Analisis Pencemaran Logam Kromium Heksavalen di Daerah Sungai pada Pertambangan Nikel. *Jurnal Pendidikan Tambusai*, *6*(2), 11978–11984.
20. Suhendara, D. T., Sachoemara, S. I., Zaidya, A. B. (2020). Hubungan kekeruhan terhadap materi partikulat tersuspensi (MPT) dan kekeruhan terhadap klorofil dalam tambak udang. *Journal of*

Fisheries and Marine Research, *4*(3), 332–338. http://jfmr.ub.ac.id

21. Tran, H. D., Nguyen, D. Q., Do, P. T., Tran, U. N. P. (2023). Kinetics of photocatalytic degradation of organic compounds: a mini-review and new approach. *RSC Advances*, *13*(25), 16915–16925. https://doi.org/10.1039/d3ra01970e
22. Wang, J., Sun, Y., Yu, M., Lu, X., Komarneni, S., Yang, C. (2021). Emulsions stabilized by highly hydrophilic TiO_2 nanoparticles via van der waals attraction. *Journal of Colloid and Interface Science*, *589*, 378–387. https://doi.org/10.1016/j.jcis.2021.01.011
23. Wei, J., Shi, P., Cui, G., Li, X., Xu, M., Xu, D., Xie, Y. (2023). Analysis of soil pollution characteristics and influencing factors based on ten electroplating enterprises. *Environmental Pollution*, *337*, 122562. https://doi.org/https://doi.org/10.1016/j.envpol.2023.122562
24. Wijayanti, M. S., Agustina, T. E., Dahlan, M. H., Teguh, D. (2023). Pengolahan Air Limbah Laboratorium Menggunakan AOPs Secara Terintegrasi. *Jurnal Ilmu Lingkungan*, *22*(1), 142–149. https://doi.org/10.14710/jil.22.1.142-149
25. Yalcin, M. (2022). The effect of pH on the physical and structural properties of TiO_2 nanoparticles. *Journal of Crystal Growth*, *585*, 126603. https://doi.org/https://doi.org/10.1016/j.jcrysgro.2022.126603
26. Zakria, H. S., Othman, M. H. D., Kamaludin, R., Sheikh Abdul Kadir, S. H., Kurniawan, T. A., Jilani, A. (2021). Immobilization techniques of a photocatalyst into and onto a polymer membrane for photocatalytic activity. *RSC Advances*, *11*(12), 6985–7014. https://doi.org/10.1039/d0ra10964a
27. Zare, E. N., Iftekhar, S., Park, Y., Joseph, J., Srivastava, V., Khan, M. A., Makvandi, P., Sillanpaa, M., Varma, R. S. (2021). An overview on non-spherical semiconductors for heterogeneous photocatalytic degradation of organic water contaminants. In *Chemosphere* 280, March, 130907. Elsevier Ltd. https://doi.org/10.1016/j.chemosphere.2021.130907